Title

X-Ray Microscopy as an Approach to Increasing Accuracy and Efficiency of Serial Block-Face Imaging for Correlated Light and Electron Microscopy of Biological Specimens

Journal

Microscopy and Microanalysis, 21(1)

ISSN

1431-9276

Authors

Bushong, Eric A
Johnson, Donald D
Kim, Keun-Young
et al.

Publication Date

2015-02-01

DOI

10.1017/s1431927614013579

Peer reviewed

HHS Public Access

Author manuscript

Microsc Microanal. Author manuscript; available in PMC 2015 April 30.

Published in final edited form as:

Microsc Microanal. 2015 February ; 21(1): 231–238. doi:10.1017/S1431927614013579.

X-ray Microscopy as an Approach to Increasing Accuracy and Efficiency of Serial Block-face Imaging for Correlated Light and Electron Microscopy of Biological Specimens

Eric A. Bushong[1], **Donald D. Johnson Jr.**[1], **Keun-Young Kim**[1], **Masako Terada**[2], **Megumi Hatori**[3,*], **Steven T. Peltier**[1], **Satchidananda Panda**[3], **Arno Merkle**[2], and **Mark H. Ellisman**[1,4]

[1]Center for Research in Biological Systems, National Center for Microscopy and Imaging Research, University of California at San Diego, 9500 Gilman Dr., La Jolla, CA 92093, USA

[2]Carl Zeiss X-ray Microscopy Inc., 4385 Hopyard Rd #100, Pleasanton, CA 94588, USA

[3]Salk Institute for Biological Sciences, 10010 N Torrey Pines Rd, La Jolla, CA 92037 USA

[4]Department of Neurosciences, University of California at San Diego School of Medicine, San Diego, La Jolla, CA 92093, USA

Abstract

The recently developed three-dimensional electron microscopic (EM) method of serial block-face scanning electron microscopy (SBEM) has rapidly established itself as a powerful imaging approach. Volume EM imaging with this scanning electron microscopy (SEM) method requires intense staining of biological specimens with heavy metals to allow sufficient back-scatter electron signal and also to render specimens sufficiently conductive to control charging artifacts. These more extreme heavy metal staining protocols render specimens light opaque and make it much more difficult to track and identify regions of interest (ROIs) for the SBEM imaging process than for a typical thin section transmission electron microscopy correlative light and electron microscopy study. We present a strategy employing X-ray microscopy (XRM) both for tracking ROIs and for increasing the efficiency of the workflow used for typical projects undertaken with SBEM. XRM was found to reveal an impressive level of detail in tissue heavily stained for SBEM imaging, allowing for the identification of tissue landmarks that can be subsequently used to guide data collection in the SEM. Furthermore, specific labeling of individual cells using diaminobenzidine is detectable in XRM volumes. We demonstrate that tungsten carbide particles or upconverting nanophosphor particles can be used as fiducial markers to further increase the precision and efficiency of SBEM imaging.

Keywords

X-ray microscopy; microcomputed tomography; serial block-face scanning electron microscopy; correlative microscopy; upconverting nanoparticles

Corresponding Author: Eric Bushong, University of California, San Diego, Biomedical Sciences Building Room 1000, 9500 Gilman Dr., La Jolla, CA 92093-0608, eric@ncmir.ucsd.edu, Phone: 858-534-7968, FAX: 858-534-7497.

*Current Address: Keio University, School of Medicine, 35 Shinanomachi Shinjyuku-ku, Tokyo 160-8582, Japan.

Introduction

Serial block-face scanning electron microscopy (SBEM) of biological specimens is a relatively new volume imaging technique that is rapidly growing in popularity throughout the biological sciences research community. Most notably, this approach is proving of great value for 3D visualization of nervous system ultrastructure, particularly when details of synaptic and other subcellular elements must be located and quantified (Holcomb, et al., 2013; Wilke, et al., 2013), but also where it is important to construct connectomic models of regional brain circuits (Helmstaedter, 2013). In addition, SBEM is increasingly used to perform nanohistology on a wide variety of tissue systems, including systems as diverse as lung (West, et al., 2010), liver (Hatori, et al., 2012), tendons (Pingel, et al., 2014), kidney (Arkill, et al., 2014), and cell cultures (Puhka, et al., 2012). Serial block-face imaging entails the iterative process of imaging a specimen block-face (usually using back-scattered electrons) followed by the removal of a thin layer of epoxy-embedded tissue from the block-face, either using ion abrasion [focused ion beam scanning electron microscopy (FIB-SEM)] (Heymann, et al., 2009; Knott, et al., 2008) or a diamond knife (Denk & Horstmann, 2004; Leighton, 1981). The current homemade or commercial systems have automated the process so that the SEM operates in SBEM mode, allowing for the collection of much larger electron microscopic (EM) volumes than could easily be collected using standard serial section transmission electron microscopy (TEM), and importantly, avoiding the section compression artifacts associated with serial section TEM (Peachey, 1958). Several reviews have compared volume EM methods, some highlighting the advantages and potential of SBEM (Kleinfeld, et al., 2011; Peddie & Collinson, 2014).

FIB-SEM and diamond knife-based SBEM are both destructive techniques, allowing only a single opportunity to collect images of an object of interest, which is usually buried within the volume of the starting specimen block. Additionally, typical experiments carried out with both techniques can require days or weeks of automated SBEM machine process time. More often in the case of diamond knife-based SBEM, data collection runs can involve months of acquisition time to obtain volumes of the scale and resolution required to contain a suitable portion of a neuronal network with adequate ultrastructural detail to assess connectivity. Consequentially, any methods that can improve the precision and efficiency of SBEM imaging would greatly enhance the power of the technique and the availability of rare imaging resources.

Nevertheless, targeting specific areas or structures for SBEM imaging presents challenges. First, as mentioned above, samples must be intensely stained with heavy metals in order to allow for back-scatter imaging of the tissue and to prevent charging artifacts in the SEM. This staining process generally results in tissue samples that are completely opaque to light, complicating efforts to find and track regions of interest (ROIs) for SBEM imaging. Second, once a sample is placed in the SEM for imaging, only the freshly prepared block-face is visible. This can create uncertainty when deciding where to collect data from the sample surface in order to reach an ROI deep within the sample accurately and efficiently. In practice it is common to collect a larger volume than necessary in order to ensure that the ROI is captured. This practice results in either wasted microscope time and/or a sacrifice in image quality due to lower resolution scans.

X-ray microscopy (XRM) is a tomographic technique that uses X-ray illumination to interrogate the interiors of optically-opaque samples in a non-destructive manner (Stock, 2009). Modern laboratory-based X-ray microscopes (XRM) are capable of producing 3D tomographic reconstructions routinely with sub-micron isotropic resolution. Numerous protocols have been developed for imaging various biological specimens with XRM (Metscher, 2009). One common approach is to stain tissue with osmium tetroxide, a stain that is presently critical for the conductive infiltration of tissue for SBEM imaging. This suggests that XRM may be capable of imaging samples prepared for SBEM. There have been initial efforts to use XRM as an intermediate step in a multiscale, correlated imaging workflow (Burnett, et al., 2014; Sengle, et al., 2013). In this report, we describe our efforts to use XRM as part of an improved SBEM correlative imaging workflow.

Materials and Methods

Sample Preparation

All animals were used according to a protocol approved by the Institutional Animal Use and Care Committee at the University of California, San Diego following AAALAC guidelines. Mice were anesthetized with ketamine / xylazine and transcardially perfused with Tyrode's solution followed by 2.5% glutaraldehyde / 2% formaldehyde in 0.15 M cacodylate buffer containing 2 mM $CaCl_2$. The brain was removed and postfixed on ice in the same fixative solution for 2 hours and then cut into 100 μm thick slices on a vibrating microtome. The slices were post-fixed at 4 °C overnight before further processing. For iontophoretic dye-filling and photooxidation, a mouse was perfused with 4% formaldehyde / 0.1% glutaraldehyde in 0.1M PBS. The brain was postfixed on ice for 2 hours and then cut into 100 μm thick slices. An astrocyte in the hippocampus was filled with 5% Lucifer yellow (LY) and then postfixed in 4% formaldehyde / 0.1% glutaraldehyde for 1 hour. LY fluorescence was imaged and the slice was bathed in 100 mM glycine-PBS buffer to quench excess aldehydes, washed with PBS, and then bathed for 5 minutes in PBS containing 0.15% 3,3'-diaminobenzidine tetrahydrochloride (DAB) and 0.1% potassium cyanide. The tissue was then illuminated with a LY filter set until LY fluorescence was replaced with light brown precipitate in transmitted light mode. The tissue was washed with PBS and then stained for SBEM imaging, as described below. For MiniSOG photooxidation, a mouse expressing MiniSOG and tdTomato in a subpopulation of retinal ganglion cells (RGCs) was transcardially perfused with 4% formaldehyde / 0.1% glutaraldehyde in 0.1M PBS. The retina was dissected and post-fixed with 4% formaldehyde in 0.1M PBS on ice for 2 hours and then cut into 100 μm thick vertical slices. The tdTomato expressed RGCs were imaged and the retina was fixed with 2.5% glutaraldehyde, 2.5mM $CaCl_2$ in 0.15 M cacodylate buffer (CB) pH 7.4, and the tissue was rinsed five times with ice-cold CB, and blocked for 30 min with 10 mM KCN, 20 mM aminotriazole, 50 mM glycine, and 0.01% hydrogen peroxide in CB. Freshly prepared DAB in CB was added to the retina, and RGCs were illuminated with 450–490 nm light from a xenon lamp for 10–15 minutes until a light brown reaction product was observed in place of the green fluorescence of MiniSOG. The tissue was then processed for SBEM.

SBEM Staining

Tissue was prepared for SBEM as previously described (Deerinck, et al., 2010). Briefly, tissue was washed with buffer and then placed into 2% OsO_4 / 1.5% potassium ferrocyanide in either 0.15M CB containing 2 mM $CaCl_2$ or 0.1M PBS for LY photooxidized specimens. The slices were left for 30 minutes on ice and then 30 minutes a room temperature. After thorough washing in double distilled water, the slices were placed into 0.5% thiocarbohydrazide for 30 minutes. The slices were again washed and then stained with 2% aq. OsO_4 for 30 min. The slices were washed and then placed into 2% aq. uranyl acetate overnight at 4 °C. The slices were washed with water at room temp and then stained with en bloc lead aspartate for 30 minutes at 60 °C. The slices were washed with water and then dehydrated on ice in 70%, 90%, 100%, 100% ethanol solutions for 10 minutes at each step. The slices were then washed twice in dry acetone and then placed into 50:50 Durcupan ACM:acetone overnight. The slices were transferred to 100% Durcupan resin overnight in vacuum chamber. The slices were then flat embedded between glass slides coated with mould-release compound and left in oven at 60 °C for 48 hours.

XRM Sample Preparation

Generally, small blocks of tissue (maximum dimension < 5mm) were cut from glass slides and then mounted with cyanoacrylate glue to the top of aluminum rods. For some samples, a rhodium-flashed copper finder grid was affixed to one face of the specimen using 5-minute epoxy (Product #14250; Devcon, Danvers, MA, USA). Alternatively, one face of the specimen was covered with a small aliquot of poly-L-lysine solution and left for 2–3 minutes. The lysine solution was briefly washed off under a stream of water and then the specimen was allowed to air dry. Tungsten (IV) carbide powder (2 μm particles; Sigma-Aldrich Corp., St. Louis, MO, USA) was temporarily suspended in distilled water by vortexing 0.1 g powder in 10 mL water. A small drop was placed on the surface of the sample previously coated with lysine. The sample was allowed to rest for 2 minutes and then wash briefly rinsed several times under a stream of distilled water and allowed to dry.

Biolistic labeling

Nanophosphor particles ($NaYSO_4$: Yb, Er) with a diameter of 1 μm were kindly provided by Intelligent Material Solutions, Inc. (San Diego, CA, USA). A 2 mg/mL solution of nanophosphor particles in 95% isopropanol/5% acetone was deposited within Tefzel tubing to create bullets for a Helios gene gun (Bio-Rad Laboratories, Hercules, CA, USA), as previously described (O'Brien & Lummis, 2011). The nanophosphor particles were shot into slices of brain tissue at 160 psi with a 2 cm distance between the tip of the gun nozzle and the tissue slice. The slice was then washed briefly in buffer, imaged by light microscopy, and subsequently processed for SBEM staining.

Light Microscopy

Prior to photooxidation, LY-filled cells were imaged on a Leica SPEII using a 63× oil objective (NA 1.30).

Brain slices containing nanophosphor particles were imaged on a Radiance 2000 microscope (Bio-Rad) equipped with a Ti-sapphire infrared laser (Spectra-Physics, Santa Clara, CA,

USA). The slices were initially imaged with a 10× objective (Nikon, NA 0.3; Chiyoda, Tokyo, Japan) with pulsed-mode illumination (980 nm) and then continuous wave illumination (980 nm), in order to collect nanophosphor and autofluorescence signal, respectively. Sub-regions were then imaged with a 40× objective (Nikon, NA 1.30) using continuous wave illumination at 980 nm, simultaneously collecting fluorescence and transmitted light images.

XRM

Most XRM work was performed on a MicroXCT-200 instrument (Zeiss X-Ray Microscopy, Pleasanton, CA, USA). This architecture combines both geometric (as found in conventional microCT constructs) and optical magnification (lens-coupled post-sample magnification) as well as optimized scintillation technologies to yield high-contrast sub-micron 3D reconstructions of a sample. XRM tilt series were generally collected at 40 kV and 4W power (100 μA current), unless otherwise noted. A Zeiss Xradia 510 Versa (Zeiss X-Ray Microscopy, Pleasanton, CA, USA) was utilized for these studies as well, as indicated in Figure 3. Collection parameters and acquisition times depend on sample geometry and resolution and are indicated in figures legends for each data set.

Serial Block-face Imaging

SBEM data was collected with a 3View unit (Gatan, Inc., Pleasanton, CA, USA) installed on a Merlin field emission SEM (Carl Zeiss Microscopy, Jena, Germany). The retinal volume was collected at 2.0 kV accelerating voltage, with a raster size of 19k × 39k and pixel dwell time of 0.5 μsec. The pixel size was 5.7 nm and section thickness was 70 nm. The astrocyte volume was collected at 2.0 kV, with a raster of 20k × 20k and pixel dwell time of 1.0 μsec. The pixel size was 4.5 nm and section thickness was 90 nm.

Image Analysis

XRM volumes were generated from XRM tilt series using XMReconstructor (Xradia). Scaling, rotation, transformation of images to find best alignment between features of interest was performed in Photoshop (Adobe Systems Inc., San Jose, CA, USA) or Imaris (Bitplane AG, Zurich, Switzerland).

2D affine transformation was performed using SciPy LinearNDInterpolator. In order to estimate the location of a target ROI on the SEM stage coordinates, fiducial markers were chosen near the ROI and their SEM stage coordinates were collected, as well as their coordinates in a previously acquired XRM volume. The two sets of coordinates were then used to calculate the SEM coordinates for the ROI based on the XRM coordinates of the ROI.

Results and Discussion

XRM Imaging of SBEM-Stained Tissue

In order to test the applicability of XRM to imaging typical SBEM samples, 100 μm thick slices of mouse brain were stained with heavy metals stains for SBEM imaging and embedded in epoxy resin (Fig 1, a,b). Following conductive infiltration with heavy metals,

the tissue was rendered completely opaque to light. Acquisition of low magnification 2D XRM projection images of the specimens was sufficient to reveal considerable detail, including basic cytoarchitecture, white matter tracts, vasculature, and cracks and other defects within the samples (Fig 1, c). The resolution achieved in XRM volumes collected at 20× (optical) magnification was sufficient to allow for the unambiguous identification of individual somata of neurons and other cell types, large dendritic processes, and occasionally nucleoli within otherwise transparent nuclei (Fig 1, d,e). Subtle differences in cytoplasmic staining were even detectable, most likely revealing interneurons typically displaying dark cytoplasm in electron micrographs.

Finder Grids for Rough Mapping of Specimens

Similar to other efforts to track ROIs within specimens from light to electron microscopy, we experimented with the use of finder grids (Auinger & Small, 2008; McDonald, et al., 2010). Quick-setting epoxy was used to fix a rhodium-plated copper finder grid to the surface of an epoxy-embedded brain slice stained for SBEM. The metal grids did not interfere with the ability to image tissue, even when the tissue was underlying an area of unmeshed metal (Fig 2). Following XRM, specimens were coated with a thin layer of gold-palladium in a sputter coater and the finder grid was carefully removed. The resulting mask image of the finder grid was visible under light microscope and in the SEM. This approach would allow an investigator to target a specific region of the tissue for acquisition of an SBEM volume.

XRM Tracking of Photooxidized Specimens

Novel transgenic probes such as MiniSOG and APEX allow for electron-dense labeling of tissue elements in a genetically targeted manner (Martell, et al., 2012; Shu, et al., 2011). To test the use of these probes with XRM imaging, retinas expressing MiniSOG and tdTomato in a subpopulation of RGC were photooxidized in the presence of DAB (Fig 3, a,b). Following SBEM staining and resin embedding, XRM imaging of the retina revealed the area of photooxidation with sufficient resolution and sensitivity to detect DAB-labeled RGC dendrites in the inner plexiform layer. In addition to detecting the DAB labeling, XRM also exposed the presence of blood vessels, tissue cytoarchitecture, and cracks in tissue, which were all useful landmarks for finding the ROI in the SEM. Based on these landmarks, an SBEM volume was collected in an area shown by XRM to contain DAB-labeled dendrites. When the XRM volume was re-sliced in an oblique orientation to match as closely as possible the cutting plane of the SBEM volume, it was possible to correlate XRM slices very closely with the block-face images collected by SBEM (Fig 3, c,d), confirming that the signals detected by XRM imaging were generated by DAB-labeled dendrites.

Tungsten Carbide as a Fiducial Marker

The retina presented a relatively simple specimen, where the search was limited to finding a ROI containing many structures of interest (i.e., RGC dendrites) along a one-dimensional aspect of the specimen (i.e., the vitreal surface of the retinal slice). Many specimens could prove much more challenging in the precision required for ROI tracking. We explored the use of small fiducial markers that would allow us to more accurately target a ROI within an SBEM sample. An astrocyte in a 100 μm-thick slice of mouse brain was iontophoretically-

filled with LY and subsequently labeled by photooxidation of DAB. The tissue was prepared for SBEM imaging using heavy metal staining and embedded in epoxy resin. Prior to performing XRM on the sample, a layer of 2 μm tungsten carbide particles was dispersed on one surface of the specimen. Following XRM reconstruction, the DAB-labeled astrocyte was clearly distinguishable within the tissue slice, as were the tungsten carbide particles at the surface (Fig 4). After the ROI was mounted on an SEM pin, it was possible to identify the tungsten carbide particles by backscatter imaging in the SEM. For several tungsten particles, the SEM stage coordinates and XRM volume coordinates were determined. Using 2D affine transformation, the SEM coordinates of the astrocyte were determined based on the XRM volume coordinates for the cell. Additionally, the XRM data revealed that the astrocyte was located approximately 45 μm beneath the surface of the epoxy resin. The SBEM microtome was used to quickly bring the block-face down to a level just above the targeted cell, thus avoiding significant acquisition time for collection of data from an area of little interest. Based on the size of the astrocyte as measured in LM and XRM volumes, an SBEM volume was collected at the coordinates calculated using the tungsten carbide fiducial markers. The resulting SBEM volume captured the astrocyte perfectly centered within the field of view, while minimizing the raster size and the time spent approaching the cell (Fig 4, d).

Nanophosphor Particles as Correlated LM-XRM-SBEM Fiducial Markers

We have also explored the use of nanophosphor particles as fiducial markers. Also known as upconverting nanoparticles, nanophosphor particles display phosphorescence emission in response to excitation with infrared wavelength light. They are available in sizes ranging from 70 nm up to 1 μm in diameter. In addition, nanophosphor emission is resistant to staining with osmium tetroxide (personal observation, data not shown).

Nanophosphor particles (1 μm diameter) were distributed within brain slices using a helium-powered biolistic device. The brain slices were imaged with 980 nm wavelength illumination in continuous wave mode to detect nanophosphor particles and in pulsed mode to image tissue autofluorescence. By combining these images, the distribution of the particles relative to tissue landmarks, such as cell layers, white matter tracts, and vasculature, was determined. The samples were then stained with the SBEM staining protocol and embedded in epoxy resin. The nanophosphor particles were easily detectable at all levels of the tissue slices in XRM volumes of the specimens. With the combination of particles characteristics and biolistic parameters used here, the majority of particles were present within the first few microns of the tissue sample, with a sizable minority having traveled completely through the specimen to the opposite surface. Few nanoparticles were found within the interior of the specimen, with most of these particles found near blood vessels. The distributions of nanophosphor particles within confocal and XRM volumes of an identical FOV were very similar, allowing for the unambiguous identification of an ROI (Fig 5).

Conclusion

We demonstrate here the ability to accurately target sub-surface volumes of interest within optically-opaque biological specimens for 3D SBEM imaging using XRM as a bridging imaging modality. Depending on the required degree of accuracy, the approach taken can be as simple as acquiring 2D projection XRM images to reveal tissue cytoarchitectural features in densely stained specimens; however, accuracy can be augmented by acquiring 3D XRM volumes of specimens with their coordinate space accurately marked using finder grids or fiducial markers. These techniques provide sufficient accuracy to allow for the targeting of single cells or even subcellular domains (e.g., a particular sub-region of a dendritic field) that have been previously imaged at lower resolution using light microscopy. Additionally, mapping a ROI with XRM greatly increases the ability to use SBEM to target structures that were previously labeled with EM dense stains using approaches such as photooxidation or Golgi labeling.

In addition to increasing the efficiency of SBEM imaging, the integration of XRM in the correlative imaging workflow offers the potential for correcting for many of the spatial distortions to biological samples that occur during specimen preparation for electron microscopy. By imaging nanophosphor particles distributed within a wet specimen and then again in the epoxy-embedded specimen, it should be possible to accurately correct for the distortions occurring within the specimen during the staining, dehydration, and resin polymerization steps. Since the ultimate goal of many SBEM studies is to reconstruct cells from large 3D volumes, the ability to correct for shrinkage and compression artifacts inherent in EM specimen preparation procedures could increase the fidelity of reconstructions.

Acknowledgements

This work was supported by an NIH National Institute of General Medical Sciences grant to Mark Ellisman (5P41GM103426).

References

Arkill KP, Qvortrup K, Starborg T, Mantell JM, Knupp C, Michel CC, Harper SJ, Salmon AH, Squire JM, Bates DO, Neal CR. Resolution of the three dimensional structure of components of the glomerular filtration barrier. BMC nephrology. 2014; 15(1) article no. 24.

Auinger S, Small JV. Correlated light and electron microscopy of the cytoskeleton. Methods in cell biology. 2008; 88:257–272. [PubMed: 18617038]

Burnett TL, McDonald SA, Gholinia A, Geurts R, Janus M, Slater T, Haigh SJ, Ornek C, Almuaili F, Engelberg DL, Thompson GE, Withers PJ. Correlative tomography. Scientific reports. 2014; 4 article no. 4711.

Deerinck T, Bushong E, Lev-Ram V, Shu X, Tsien R, Ellisman M. Enhancing serial block-face scanning electron microscopy to enable high resolution 3-D nanohistology of cells and tissues. Microscopy and Microanalysis. 2010; 16(SupplementS2):1138–1139.

Denk W, Horstmann H. Serial block-face scanning electron microscopy to reconstruct three-dimensional tissue nanostructure. PLoS biology. 2004; 2(11):e329. [PubMed: 15514700]

Hatori M, Vollmers C, Zarrinpar A, DiTacchio L, Bushong EA, Gill S, Leblanc M, Chaix A, Joens M, Fitzpatrick JA, Ellisman MH, Panda S. Time-restricted feeding without reducing caloric intake prevents metabolic diseases in mice fed a high-fat diet. Cell metabolism. 2012; 15(6):848–860. [PubMed: 22608008]

Helmstaedter M. Cellular-resolution connectomics: challenges of dense neural circuit reconstruction. Nature methods. 2013; 10(6):501–507. [PubMed: 23722209]

Heymann JA, Shi D, Kim S, Bliss D, Milne JL, Subramaniam S. 3D imaging of mammalian cells with ion-abrasion scanning electron microscopy. Journal of structural biology. 2009; 166(1):1–7. [PubMed: 19116171]

Holcomb PS, Hoffpauir BK, Hoyson MC, Jackson DR, Deerinck TJ, Marrs GS, Dehoff M, Wu J, Ellisman MH, Spirou GA. Synaptic inputs compete during rapid formation of the calyx of Held: a new model system for neural development. The Journal of neuroscience : the official journal of the Society for Neuroscience. 2013; 33(32):12954–12969. [PubMed: 23926251]

Kleinfeld D, Bharioke A, Blinder P, Bock DD, Briggman KL, Chklovskii DB, Denk W, Helmstaedter M, Kaufhold JP, Lee WC, Meyer HS, Micheva KD, Oberlaender M, Prohaska S, Reid RC, Smith SJ, Takemura S, Tsai PS, Sakmann B. Large-scale automated histology in the pursuit of connectomes. The Journal of neuroscience : the official journal of the Society for Neuroscience. 2011; 31(45):16125–16138. [PubMed: 22072665]

Knott G, Marchman H, Wall D, Lich B. Serial section scanning electron microscopy of adult brain tissue using focused ion beam milling. The Journal of neuroscience : the official journal of the Society for Neuroscience. 2008; 28(12):2959–2964. [PubMed: 18353998]

Leighton SB. SEM images of block faces, cut by a miniature microtome within the SEM - a technical note. Scanning electron microscopy. 1981; (Pt 2):73–76. [PubMed: 7323733]

Martell JD, Deerinck TJ, Sancak Y, Poulos TL, Mootha VK, Sosinsky GE, Ellisman MH, Ting AY. Engineered ascorbate peroxidase as a genetically encoded reporter for electron microscopy. Nature biotechnology. 2012; 30(11):1143–1148.

McDonald K, Schwarz H, Muller-Reichert T, Webb R, Buser C, Morphew M. "Tips and tricks" for high-pressure freezing of model systems. Methods in cell biology. 2010; 96:671–693. [PubMed: 20869543]

Metscher BD. MicroCT for comparative morphology: simple staining methods allow high-contrast 3D imaging of diverse non-mineralized animal tissues. BMC physiology. 2009; 9 article no. 11.

O'Brien JA, Lummis SC. Nano-biolistics: a method of biolistic transfection of cells and tissues using a gene gun with novel nanometer-sized projectiles. BMC biotechnology. 2011; 11 article no. 66.

Peachey LD. Thin sections. I. A study of section thickness and physical distortion produced during microtomy. The Journal of biophysical and biochemical cytology. 1958; 4(3):233–242. [PubMed: 13549493]

Peddie CJ, Collinson LM. Exploring the third dimension: Volume electron microscopy comes of age. Micron. 2014; 61C:9–19. [PubMed: 24792442]

Pingel J, Lu Y, Starborg T, Fredberg U, Langberg H, Nedergaard A, Weis M, Eyre D, Kjaer M, Kadler KE. 3-D ultrastructure and collagen composition of healthy and overloaded human tendon: evidence of tenocyte and matrix buckling. Journal of anatomy. 2014; 224(5):548–555. [PubMed: 24571576]

Puhka M, Joensuu M, Vihinen H, Belevich I, Jokitalo E. Progressive sheet-to-tubule transformation is a general mechanism for endoplasmic reticulum partitioning in dividing mammalian cells. Molecular biology of the cell. 2012; 23(13):2424–2432. [PubMed: 22573885]

Sengle G, Tufa SF, Sakai LY, Zulliger MA, Keene DR. A correlative method for imaging identical regions of samples by micro-CT, light microscopy, and electron microscopy: imaging adipose tissue in a model system. The journal of histochemistry and cytochemistry : official journal of the Histochemistry Society. 2013; 61(4):263–271. [PubMed: 23264636]

Shu X, Lev-Ram V, Deerinck TJ, Qi Y, Ramko EB, Davidson MW, Jin Y, Ellisman MH, Tsien RY. A genetically encoded tag for correlated light and electron microscopy of intact cells, tissues, and organisms. PLoS biology. 2011; 9(4):e1001041. [PubMed: 21483721]

Stock, SR. Microcomputed Tomography: Methodology and Applications. Boca Raton, FL: CRC Press; 2009.

West JB, Fu Z, Deerinck TJ, Mackey MR, Obayashi JT, Ellisman MH. Structure-function studies of blood and air capillaries in chicken lung using 3D electron microscopy. Respiratory physiology & neurobiology. 2010; 170(2):202–209. [PubMed: 20038456]

Wilke SA, Antonios JK, Bushong EA, Badkoobehi A, Malek E, Hwang M, Terada M, Ellisman MH, Ghosh A. Deconstructing complexity: serial block-face electron microscopic analysis of the hippocampal mossy fiber synapse. The Journal of neuroscience : the official journal of the Society for Neuroscience. 2013; 33(2):507–522. [PubMed: 23303931]

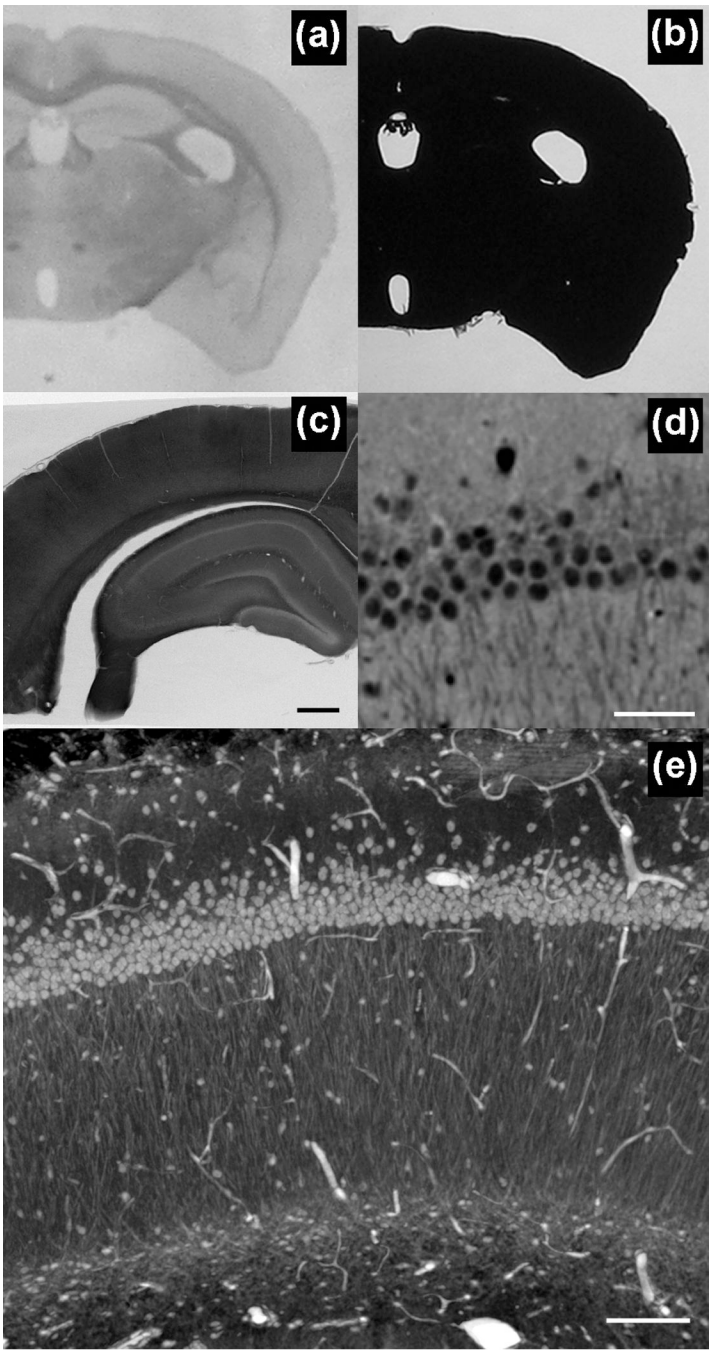

Figure 1.

XRM allows for high-resolution imaging of tissue stained for SBEM. (a,b) While it is possible to easily identify anatomical features within a brain slice using light microscopy, the tissue is completely opaque to light following staining for SBEM. (c) A 2D projection image with the XRM using a 4× objective and 40 kV reveals details within the SBEM-stained tissue slice, including cell layers, vasculature, and white matter tracts. (d) A virtual 2D slice from a XRM volume allows for the discrimination of individual cells, dendrites, dark neurons, and nucleoli. The volume was collected with a 20× objective and using a 180°

sample rotation and 0.1° tilt increments and 15 sec exposures (~7.5 hours total). (e) A 3D ray trace projection image of the same volume. Scale bar: (c) 500 μm, (d) 50 μm, and (e) 100 μm.

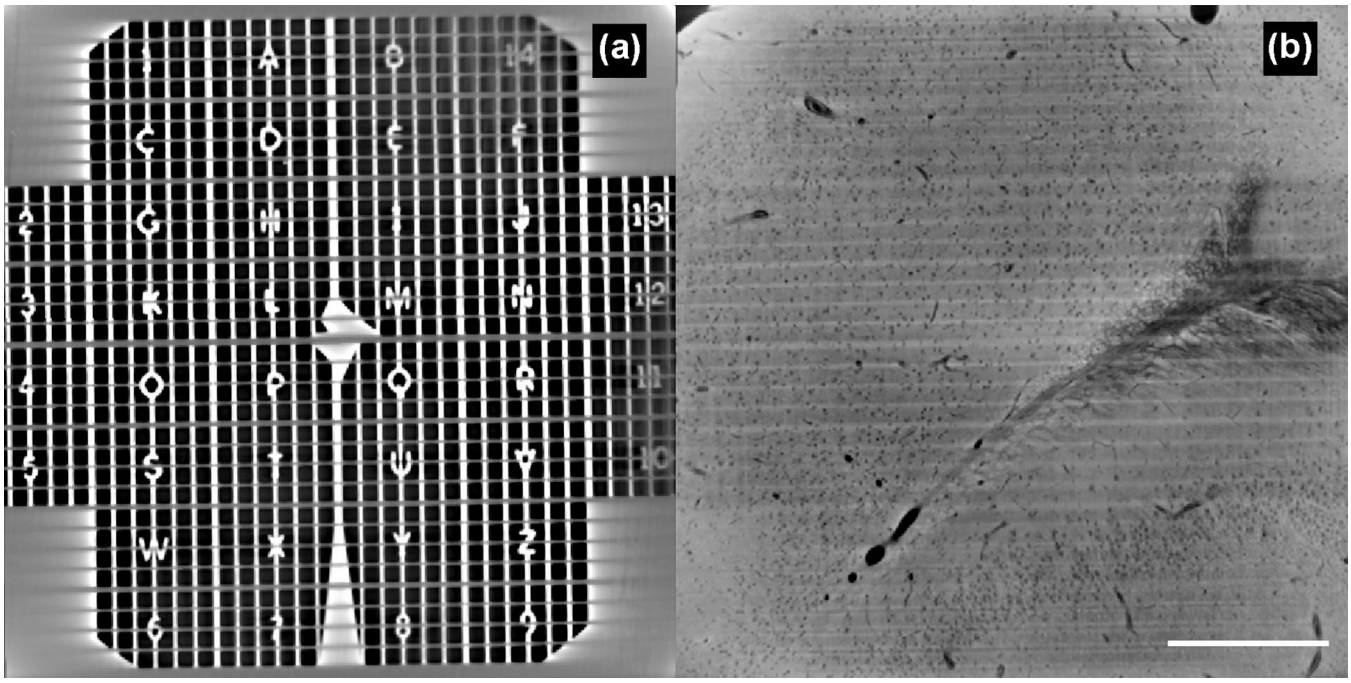

Figure 2.

Finder grids are a simple method for tracking ROIs between XRM and SBEM modalities. (a) An EM finder grid was attached to the surface of a resin-embedded, SBEM stained slice of brain tissue. The grid landmarks are clearly visible in a computed slice from a XRM volume. (b) A second computed slice taken through the tissue shows that tissue structures are visible even in areas laying under areas of solid metal in the finder grid. The volume was collected using a 10× objective, with a 360° sample rotation at 0.2° tilt increments and 8 sec exposures (~4 hours total). Scale bar is 500 μm.

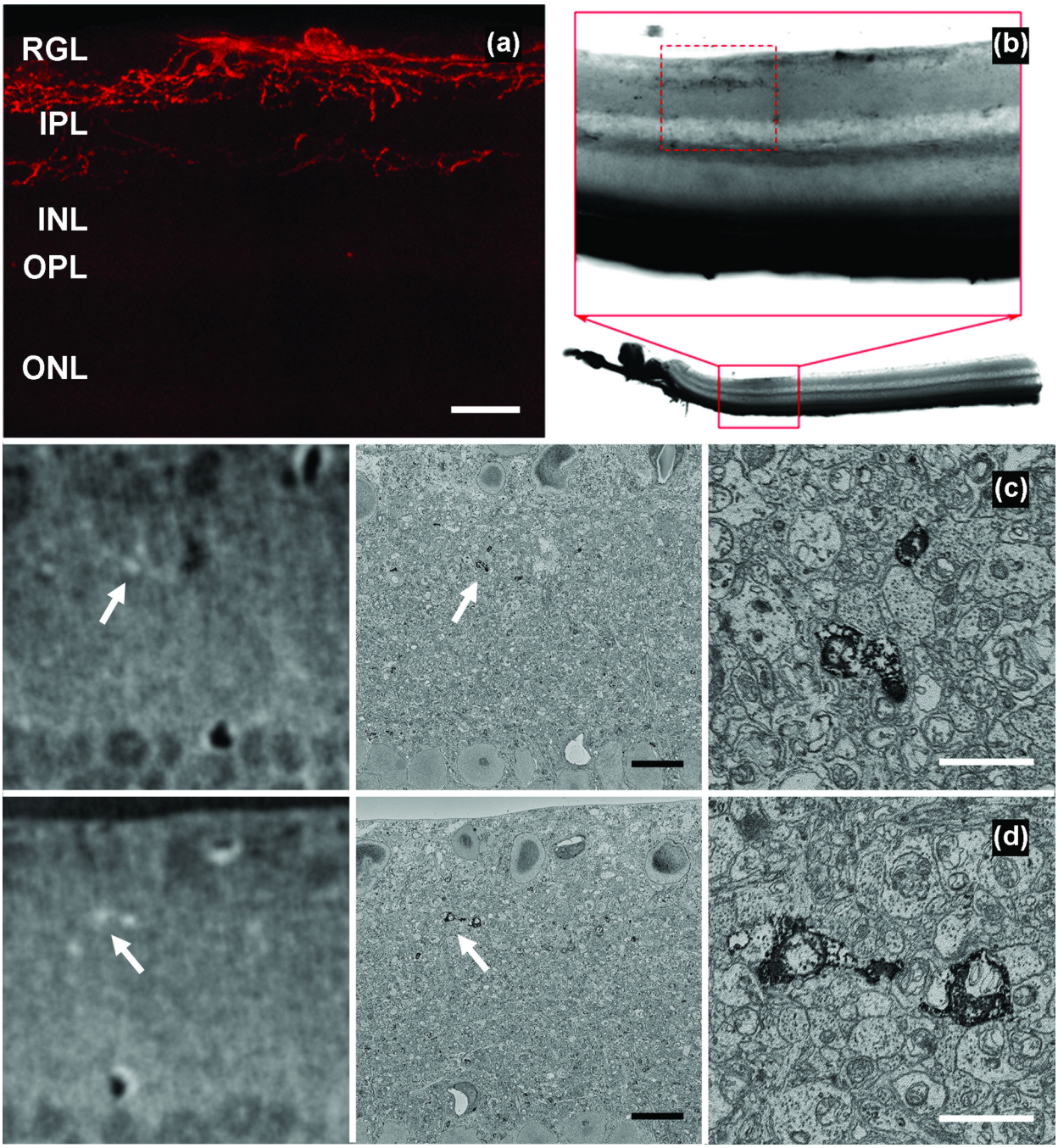

Figure 3.

Specific-labeled of structures for EM is also visible in XRM volumes following staining for SBEM. (a) tdTomato labeling of RGC co-expressing MiniSOG. RGL: retinal ganglion cell layer, IPL: inner plexiform layer, INL: inner nuclear layer, OPL: outer plexiform layer, ONL: outer nuclear layer (b) Light microscopic image of the retina following photooxidation. Small area containing DAB-filled dendrites, corresponding to area in (a) is marked with dashed box. (c,d) Bright spots in XRM volume (arrows in left panels) from same area in (a) and (b) correspond to DAB-labeled dendrites in SBEM images (arrows in

center panel, higher magnification in right panels). The XRM volume was collected using a ZEISS Xradia 510 Versa at 40 kV and 3 W power, 180° sample rotation at 0.1° tilt increments, with 10 sec exposure time (~6 hours total). Scale bar: (a) 50 μm, (c,d center panels) 10 μm, (c,d right panels) 2.5 μm.

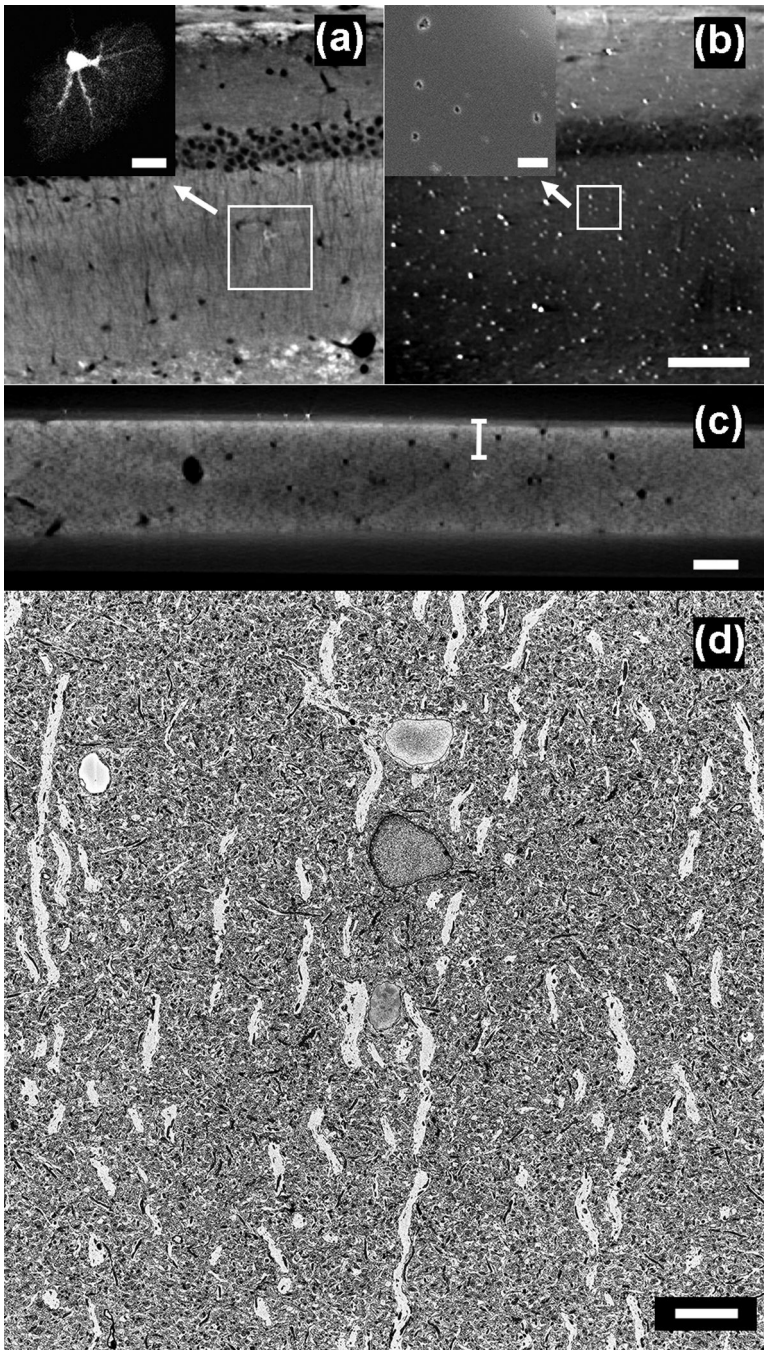

Figure 4.

Tungsten carbide particles are effective fiducial markers for precisely tracking ROIs from XRM to SBEM. (a) A photooxidized astrocyte in tissue stained for SBEM is visible in a computed slice from a XRM. Inset shows a confocal image of the astrocyte prior to photooxidation. XRM volume was collected at 20 kV and 2W power, with a 20× objective using 180° sample rotation with 0.1° tilt increments and 25 sec exposures (~13 hours total). (b) Another computed slice from the same volume shows the distribution of tungsten carbide particle on one surface of the sample. Inset shows SEM image of area in white box in (b),

with several tungsten carbide particles visible. (c) Computed slice through cross section of the sample allows for determination of the depth of the astrocyte within the specimen. (d) SBEM slice taken from volume collected of the astrocyte, based on the coordinates calculated using tungsten carbide particles. The astrocyte is properly centered in field of view. Scale bar: (a inset) 15 μm, (b inset) 4 μm, (b) 100 μm, (c) 50 μm, (d) 10 μm.

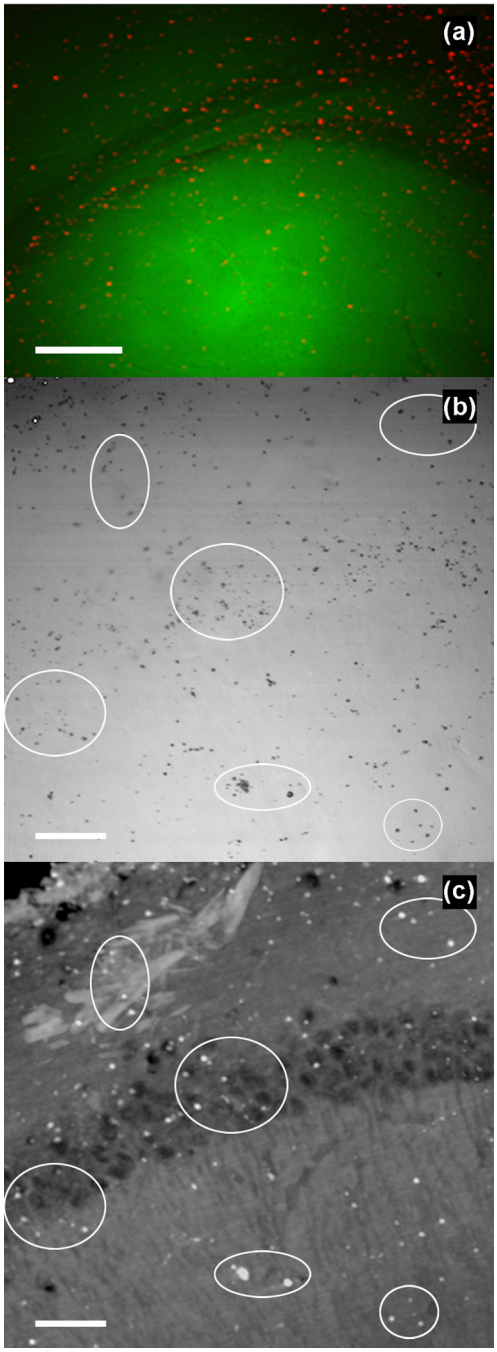

Figure 5.

Nanophosphor particles are useful fiducial particles that can also be used to correlate ROIs between LM and XRM. (a) Nanophosphor particles (red) are distributed across a brain slice (green) using a gene gun. (b) Transmitted light image of nanophosphor particles on one surface of a brain slice. (c) Computed slice from XRM volume of same field of view as in (b). Volume was collected with 20× objective using 360° sample rotation with 0.2° tilt increments and 15 sec exposures (~7.5 hours total). Scale bar: (a) 200 μm, (b,c) 50 μm.